Accepted Manuscript

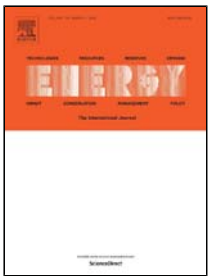

HIGH-TEMPERATURE PCM-BASED THERMAL ENERGY STORAGE FOR INDUSTRIAL FURNACES INSTALLED IN ENERGY-INTENSIVE INDUSTRIES

Patricia Royo, Luis Acevedo, Victor J. Ferreira, Tatiana García-Armingol, Ana M. López-Sabirón, Germán Ferreira

PII:	S0360-5442(19)30317-2
DOI:	10.1016/j.energy.2019.02.118
Reference:	EGY 14760
To appear in:	*Energy*
Received Date:	26 November 2018
Accepted Date:	16 February 2019

Please cite this article as: Patricia Royo, Luis Acevedo, Victor J. Ferreira, Tatiana García-Armingol, Ana M. López-Sabirón, Germán Ferreira, HIGH-TEMPERATURE PCM-BASED THERMAL ENERGY STORAGE FOR INDUSTRIAL FURNACES INSTALLED IN ENERGY-INTENSIVE INDUSTRIES, *Energy* (2019), doi: 10.1016/j.energy.2019.02.118

This is a PDF file of an unedited manuscript that has been accepted for publication. As a service to our customers we are providing this early version of the manuscript. The manuscript will undergo copyediting, typesetting, and review of the resulting proof before it is published in its final form. Please note that during the production process errors may be discovered which could affect the content, and all legal disclaimers that apply to the journal pertain.

ACCEPTED MANUSCRIPT

HIGH-TEMPERATURE PCM-BASED THERMAL ENERGY STORAGE FOR INDUSTRIAL FURNACES INSTALLED IN ENERGY-INTENSIVE INDUSTRIES

Patricia Royo[1], Luis Acevedo [1], Victor J. Ferreira [1], Tatiana García-Armingol [1], Ana M. López-Sabirón [1], Germán Ferreira [1*]

[1]Research Centre for Energy Resources and Consumption (CIRCE), CIRCE Building – Campus Río Ebro, Mariano Esquillor Gómez, 15, 50018, Zaragoza, Spain

e-mail: proyo@fcirce.es

e-mail: lacevedo@fcirce.es

e-mail: vferreira@fcirce.es

e-mail: tgarcia@fcirce.es

e-mail: amlopezs@fcirce.es

[*]e-mail: gferreira@fcirce.es

Keywords: Phase change materials; High-temperature thermal energy storage; Energy-intensive industries; Waste heat recovery; Heat transfer model simulation.

Abstract

The energy considered as waste heat in industrial furnaces owing to inefficiencies represents a substantial opportunity for recovery by means of thermal energy storage (TES) implementation. Although conventional systems based on sensible heat are used extensively, these systems involve technical limitations. Latent heat storage based on phase change materials (PCMs) results in a promising alternative for storing and recovering waste heat. Within this scope, the proposed PCM-TES allows for demonstrating its implementation feasibility in energy-intensive industries at high temperature range. The stored energy is meant to preheat the air temperature entering the furnace by using a PCM whose melting point is 885°C. In this sense, a heat transfer model simulation is established to determine an appropriate design based on mass and energy conservation equations. The thermal performance is analysed for the melting and solidification processes, the phase transition and its influence on heat transference. Moreover, the temperature profile is illustrated for the PCM and combustion air stream. The obtained results prove the achievability of very high temperature levels (from 700 to 865°C) in the combustion air preheating in a ceramic furnace; so corroborating an energy and environmental efficiency enhancement, compared to the initial condition presenting an air outlet at 650°C.

HIGHLIGTHS

- A thermal energy storage based on PCM is proposed to recover high temperature heat.
- An energy intensive industry study case reached a temperature increase up to 200°C.
- 3D-numerical model assesses the thermal behaviour of the waste heat recovery system.
- Combustion air temperature profiles are analysed during charging and discharging.
- A basis is set for system design, thermal stress resistance and material selection.

1 Introduction

Over the past century, awareness of the environmental sustainability principle has been increasing worldwide and has become deeply rooting in the culture of companies and industries. At present, numerous compromises and initiatives aim at boosting the key performance guidelines in order to meet environmental targets [1]. In particular, the energy-intensive industry (EII), which is composed of aluminium, cement, steel, ceramic, glass and chemical industries, among others, is making significant efforts to decarbonise their sectors following the 2050 roadmap for energy [2], while being economically competitive. However, it is not straightforward to achieve an industrial sector with zero carbon dioxide emissions and strong commitment is required in order to construct a plan for a low carbon society. EII is facing major challenges to avoid dangerous anthropogenic interference with the climate system; for example, by achieving the global warming target of 'well under 2 degrees Celsius' expressed in the Paris Agreement [3]. To this end, the key actions are focused on implementing clean energy policies, renewable energy integration, switching to alternative fuels, removing carbon dioxide from the atmosphere by means of sequestration, developing advanced materials, integrating energy storage and adopting the superior available technologies [4, 5], all under a lifecycle product approach. All of these strategies arise as promising actions to improve energy and resources efficiency, optimise production processes, reduce heat losses and minimise residues [6]. In particular, the integration of energy transformation and recovery is emphasised in order to avoid unnecessary entropy production, while causing the production processes to be more cost-effective and environmentally friendly [7]. This concept approach of integration, flexibility and symbiosis is defined as Smart Energy System, according to H. Lund *et al.* [8].

The industrial sector accounts for one third of the total energy consumed in society, of which a substantial part eventually becomes waste heat owing to inefficiencies. The average thermal efficiency for installed industrial furnaces is approximately 60% [9], which represent a significant opportunity for improvement by reducing the main causes of heat losses in industrial furnaces, namely leaking of exhaust gases, poor insulation and inefficient performance of combustion parameters. Applying the best available technology in industry can involve a 25% decrease in the energy intensity; even more, an addition 20% can be achieved through innovative systems [8]. Within this context, industrial manufacturing plants are highly appropriate for integrating technologies for waste heat recovery. Furnaces heated by the combustion of hydrocarbon fuels; that is, natural gas, exhibit important heat losses in flue gases (with an average value of 40%, although very poor performances may increase the heat losses up to 70%) [10]. In Europe alone, this heat recovery potential has been estimated as more than 300 TWh per year [11], which would imply a reduction of 250 million tonnes of CO_2 emissions per year.

Despite the improvement that recovering waste heat provides to the industries, it is limited by technology and finance difficulties [12]. The implementation of new equipment usually requires high investment as well as an in-depth renovation process. Manufacturing plants are long lasting, offering few opportunities for upgrades to the energy efficiency of the core process [13]. This constraint may be overcome by means of retrofitting strategies based on the refurbishment of existing equipment. Retrofitting actions are mainly aimed at the cost optimisation of an already existing plant, adaptation of plant components for new products, achievement of more efficient and sustainable processes and a reduction in energy and resources consumption [6]. However, these alternatives are not always possible, as there may be lifespan, cost and space restrictions in the plant. Thus, benefits and costs must be thoroughly assessed in order to identify the most

profitable and efficient alternative.

The working temperature range of the EII achieves very high levels, as illustrated in Figure 1, which is based on a report by the Bureau of Energy Efficiency [14]. The most common waste heat streams may be gases (including exhaust gas, flaring gas, steam and hot air), liquids (such as hot oil and refrigeration water) and solids (for example, waste and products) [15]. Examples of typical heat sources in which it is possible to find these streams are melting and heating furnaces, boilers, incinerators, thermal treatments and steam distributions. All of these represent the possibility to recover considerable amounts of heat, which is otherwise wasted or simply released to the environment. The wasted heat can be recovered and reused, either inside or outside the process or even the plant, for different purposes in the functioning of each production process and depending on the heat quality. For example, the most common uses are combustion air preheating, charge preheating prior to entering the furnace and supplying energy to other upstream and downstream processes.

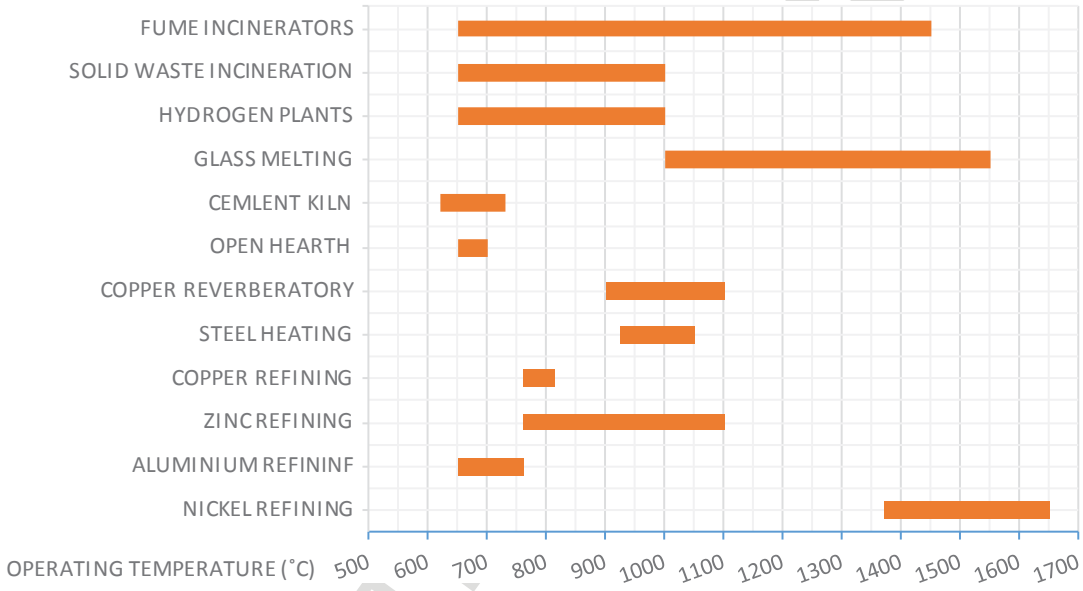

Figure 1. Typical operating temperature range of different energy-intensive industry processes (adapted from data reported in [14]).

In light of the above, thermal energy storage (TES) can be applied as either a new integrated or a retrofitting element for recovering waste heat in EII. TES has been proven as an indispensable approach to improving the energy efficiency of different systems, and consequently, both the primary fuel consumption and environmental impact can be reduced [16]. The major technologies for TES include sensible heat, latent heat and thermochemical systems [17]. Latent heat systems are based on phase change materials (PCMs), owing to their property of releasing or absorbing energy while changing their physical state, usually from solid to liquid, and vice versa. The PCM turns into liquid as it absorbs thermal energy, while the stored thermal energy is released during the solidification phase. Compared to other technologies, PCM is distinguished by its higher energy storage density, storing thermal energy at a constant temperature, increasing the system flexibility and exhibiting acceptable long-term reliability [18]. PCMs use the solid/liquid phase transition to store thermal energy based on their latent heat capacity. This particularity allows PCMs to store between 5 and 100 times more energy than sensible heat systems with the same volume [19, 20]. For a certain application, the operating temperature of the heat transference should match the PCM transition temperature. A wide variety of PCMs are already available and

applicable in various fields [20, 21], such as solar technology, water and air heating, buildings, heat exchangers, thermal storage, textiles, medicine, transportation, food and beverage, and thermal preservation.

These materials are classified as organic, inorganic and eutectic [22], depending on the material nature. Organic materials are normally more suitable for operating temperatures below 100˚C; otherwise, inorganic materials (salts and metals) may fulfil higher temperature requirements (up to 1680˚C [23]). Thus, this group and its eutectic mixed variety offer adequacy for developing applications in the EII sector [24]. However, despite the advantages offered by these materials, considerable challenges must still be overcome, such as corrosion, reactivity, compatibility, structural resistance and safety issues. Even though these materials have been tested at the laboratory scale [20, 25-27], their applications are scarce at industrial levels, and very few materials meeting these requirements have been fully commercialised.

Most of the applications have been found in hot water or steam generation processes in solar plants [28-32]. Y. Lin *et al.* [12] highlighted the existing gap between theoretical researches and practical operations. Furthermore, there remains a lack of research owing to the mentioned technical and economic implications under real conditions, no reports in the assessment of the energy savings and an unclear knowledge about the PCM thermal performance at high temperatures in industrial applications [33]. It is even more complicated to find results at higher temperature ranges, since only a few demonstrators of high-temperature LHS has been constructed and operated over 200 °C, due to the high cost of experimental test and model validation with experimental data under real conditions [34]. Therefore, there exists a clear need, which the present work aims at contributing, to establish computational models for predicting the thermal behaviour of PCM-TES working under real operational conditions. Accomplishing an appropriate design and material selection is of paramount importance for storage systems at such high temperatures.

Thus, the main aim of this study is to address the previous issues in order to expand the PCM-TES incorporation into the EII sectors at high temperature levels. This research intends to make advances towards PCM-TES industrial applicability, in order to overcome the performance of conventional commercial sensible heat solutions, which are limited in recovering high-temperature heat [36]. To achieve this, it is necessary a detailed evaluation of the PCM-TES system performance which is proposed to recover high temperature waste heat from an exhaust gas stream at around 1100 ˚C. Furthermore, the use of PCM results in non-linearity of the enthalpy-temperature function, which severely limits the application of conventional design methods [35]. To solve this, a computer-aided design based on an own developed 3D model is applied to a case study in the ceramic sector, as one of the most relevant within the European EII. The simulation results allow performing an appropriate design in material and sizing, ensuring the technical feasibility of this kind of systems working at critical temperature ranges. In addition, this modelling could predict the feasibility and potential implications of the system as a first stage, supporting the design of the PCM-based heat recovery system and decreasing the uncertainty level prior to developing a more optimised and detailed approach. The results aim at representing the thermal performance during the PCM phase transition by means of temperature profiles, and also describe the combustion air temperature during the charge and discharge processes.

2 Methods

2.1 System requirements

A case study in a ceramic production plant belonging to the EII is considered, as considerable wasted heat can be identified in this sector. In the ceramic sector, frits are the main component of almost all ceramic glazes, which are a homogeneous mixture of a variety of inorganic materials resulting from a melting process in a fusion furnace at a high-temperature, followed by rapid quenching. Finally, the frits are dried with air and an ulterior milling process is applied to convert them into small glass particles. Therefore, a large quantity of hot flue gases at around 1100 ˚C is generated from the furnace. Within this context, the PCM-TES integration aims at recovering heat from these high-temperature exhaust gases in order to preheat the combustion air entering the frit furnace (around 850 ˚C), as depicted in Figure 2. In the present case, although a conventional sensible heat exchanger exists at the plant, there remains potential value for heat recovery. Moreover, if the industry does not use any type of heat recovery system, the potential would be greater, as would the energy and resources savings.

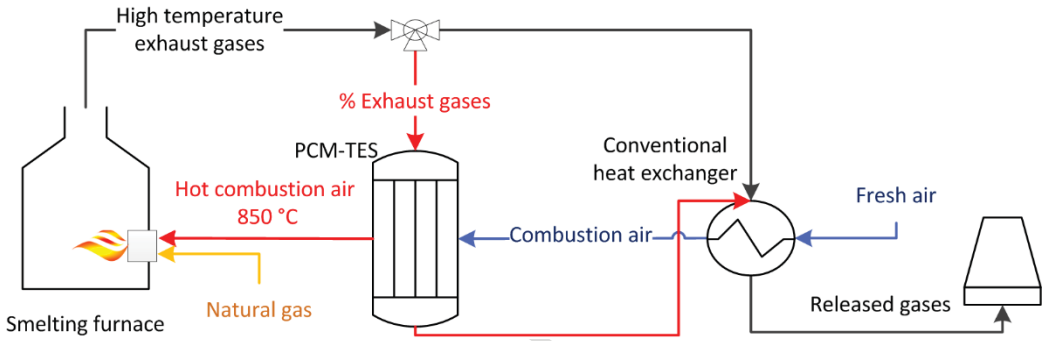

Figure 2. Diagram for PCM-TES integration for heat recovery in an industrial plant.

Firstly, the heat demand (Q) of the combustion air preheating is quantified in order to determine the PCM-TES system storage capacity. In Eq. (1), $m_{comb.air}$ is the mass flow, c_p is the specific heat and $\Delta T_{comb.air}$ is the gradient from the combustion air. Assuming no losses in the storage system, the heat demand in the combustion air sets the requirement for the amount of PCM required to store the heat.

$$Q = m_{comb.air} \cdot c_p \cdot \Delta T_{comb.air} \tag{1}$$

Regarding the PCM selection, several alternative PCMs underwent a comparison process [37], weighting the advantages and disadvantages in order to reach a suitable decision for the specific application. The expected outlet temperature should approximately correspond to the selected PCM melting point. This temperature must be defined in the highest possible range in order to absorb high-quality heat (high exergy), so it is more valuable in upstream or downstream processes. The selected PCM is a commercial inorganic molten salt, which is highlighted by its high latent heat capacity (properties described in Table 1). This salt is the only option available at such high temperatures on a technical and commercial level [12]. Molten salts are widely used as TES materials in the industry because of its higher decomposition temperature [38]; however, the low thermal conductivity may result in long-lasting charge/discharge processes.

The heat transferred in the PCM (Q_{PCM}) on either sides of the tube during the charge/discharge process is governed by the log mean temperature difference method [35] between the heat transfer fluid (HTF) and PCM, as described by Eq. (2). This methodology strongly depends on the PCM-TES configuration and design, since it evaluates the heat transfer as a function of $\Delta T_{HTF\text{-}PCM}$, which is the temperature difference between the inlet/outlet HTF and PCM melting temperature, heat exchange area (A) and global heat transfer coefficient (U). The overall heat transfer coefficient is calculated as the sum of the HTF thermal resistances, wall tube and PCM, with the phenomena of convection and conduction.

$$Q_{PCM} = U \cdot A \cdot \Delta T_{HTF-PCM} \quad (2)$$

2.2 System description

In this specific case, the proposed configuration to be analysed is a shell and tube system. This configuration is among the most commonly used [39-41], owing to its robust construction geometry, as well as ease of maintenance, disassembly and possibility for future upgrades. Furthermore, in the shell and tubes systems, heat losses are minimal and the heat transference is enhanced along the PCM tubes [42, 43]. The system is composed of seven double concentric tubes embedded in a shell with a 2 m diameter and 3.5 m length. The double concentric tube design sets the suitable arrangements considering the quantity and quality of the waste heat sources, defining the basic sizing and operational parameters of the PCM-TES, following the above methodology. Besides this configuration allows the disassembly for maintenance labours or PCM replacement, if needed. A summary of the most relevant parameters of the PCM-TES solution and main PCM thermo-physical properties is provided in Table 1.

Table 1. Main design parameters and thermal-physical properties of PCM-TES.

PCM-TES parameters/properties	Value and units
System configuration	Shell and tube
Number and type of tubes	7 double-concentric
Tube length filled with PCM	3.5 m
Tube / Shell diameter	0.6 m / 2 m
System material	Ni-based alloys, stainless steels
PCM type	Inorganic, molten salt
PCM Melting temperature	885 ˚C
PCM mass	4700 kg
PCM latent heat of fusion	236 kJ/kg
PCM thermal conductivity	0.6 W/(m·K)
Metal tube conductivity	25.6 W/(m·K)
System storage capacity	300 kWh

During the charging, the flue gases move through the innermost part of the double concentric tube to transfer the heat to the PCM, as detailed in Figure 3. The convective heat transfer coefficient for the tube side is calculated according to Eq.(3) and it takes into account both thermomechanical properties of the materials (such as the thermal conductivity k and the Nusselt number (Nu)) and the representative geometrical parameters (D) [44].The convection inside the tubes influences the charging process and it is defined by the flue gas stream (h_{fg}=6.9 W/(m^2·K)). The PCM inside the

tubes absorbs the heat and starts increasing its temperature until it reaches the phase-change point. During the phase transition, the heat is stored by conduction (k) in function of the latent heat capacity; while the PCM becomes liquid. The PCM ring thickness will be set considering the technical aspects in order to ensure suitable thermal transference. This process lasts until almost all the PCM is completely melted. After that, the flue gas stream through the PCM-TES is closed and the air combustion starts flowing through the shell during the discharging. Then, the PCM becomes solid again while releasing the heat, thus increasing the temperature of the combustion air stream, which is flowing through the external shell. In this case, the discharging phase is governed by the combustion air streaming in counter flow inside the shell. The equation for calculating the convective coefficient through the shell is defined by Eq.(4) [44], corrected with the baffle pitch factor (h_{ca}=67.2 W/(m^2·K)); where Re and Pr correspond to the Reynolds and Prandtl number, correspondingly.

$$h_{fg} = \frac{k \cdot Nu}{D} \tag{3}$$

$$h_{ca} = \frac{k}{D} \cdot 0.36 \cdot Re^{0.55} \cdot Pr^{1/3} \tag{4}$$

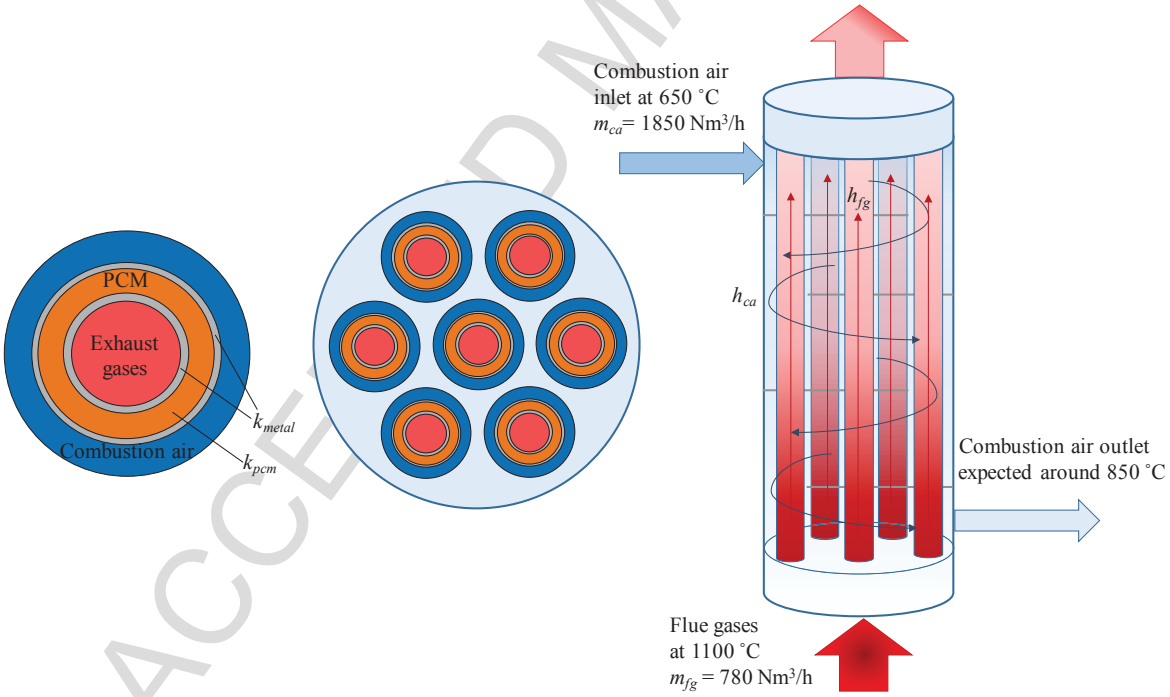

Figure 3. Diagram of PCM-TES input/output streams, cross-section and tube configuration.

Figure 3 gathers the information related to the PCM-TES configuration, the heat source temperatures and flows, and the target preheating in the combustion air after moving through the PCM-TES. The tubes are distributed in a triangular arrangement, as depicted in the cross-section. In this manner, the air turbulence through the shell is greatest, and the shell diameter is smaller than in a rectangular arrangement [45]. Moreover, the use of baffles attached to the shell side with

a minimum pitch of 15% along the tube is suggested in order to support the tube bundle and direct the flow inside the shell. The baffles enhance the mechanical stability of the overall system and extend the residence time of the fluid to be heated, thereby increasing the heat transference and final outlet temperature achieved. Moreover, it is advisable to install the PCM-TES in a vertical position, because this offers improved mechanical stress resistance, easier cleaning and acceleration of the melting process compared to the horizontal orientation. The main reason for the difference of performance in time is the effect of gravity on the system, which induces a larger portion of natural convection.

2.3 Numerical model for PCM system

2.3.1 Governing equations

During the design phase, one of the most commonly used methodologies is simulation tools based on numerical models [35]. These allow for the generation of representative results considering boundary conditions associated with the operating conditions of the real process in which the PCM system is intended to be coupled. Simulation code in MATLAB® software was developed based on a numerical model, to obtain both the temperature profile and phase change performance along the charge/discharge cycles. A three-directional finite differences method (FDM) is selected to solve the heat equation in the transient state with stair-step modification [46], increasing the mesh points in the radius vicinity [47], which allows for an appropriated adaptation for these geometries. The analysis of the method accuracy reported in reference [48] shows that the incurred errors can be ignored in applications where the boundary is not the focus of the simulation, as in the present case. Furthermore, the advantages over other methods are easier programming, as well as less memory resources and iteration time required. The heat conduction and convection are investigated and considered within this model; while radiation was neglected due to practical issues. This 3D model is the core of the computer-aided design, which allows adapting the main parameters to achieve a suitable PCM solution for each specific study case.

In order to solve the complete model, calculation of the temperature profile (T) is presented in the main equation, Eq. (5), for three dimensions, in accordance with the studies of S. Mazumder [49] and Ferziger [46]. An adiabatic system is considered, where ρ is the density, κ refers to the equivalent thermal conductivity and ∂t is the time variation:

$$\rho \cdot c_p \frac{\partial T}{\partial t} = \kappa \left(\frac{\partial^2 T}{\partial x^2} + \frac{\partial^2 T}{\partial y^2} + \frac{\partial^2 T}{\partial z^2} \right) \quad (5)$$

Regarding the boundary conditions of Eq. (5), the internal and external tube walls are governed by the convection heat transfer inside and outside the tube, where each HTF (exhaust gases and combustion air) flows. At the beginning of the simulation (first charge) all surfaces are assumed to be at ambient temperature. During the performance of a cycle, the charging ends when the PCM melted percentage achieves more than 90%. At that point, the calculated temperature profiles set the initial conditions for the discharge process and the temperature at the flue gas outlet is also calculated. During this stage, the new temperature profiles for the PCM are calculated, as well as the combustion air outlet temperature. The discharge phase should last for as long as there is an increase with respect to the combustion air without PCM-TES integration (650˚C). Hence, the minimum limit for acceptable discharging is fixed at 700˚C. Finally, when

the discharging is finished, the resulting temperature profiles becomes the initial conditions for the next cycle.

In the simulation, the temperature discretisation applied for an internal node is illustrated in Eq. (6) [50], where τ is the Fourier number.

$$T_{(i,j,k)}^{n+1} = \tau\left(T_{(i+1,j,k)}^{n} + T_{(i-1,j,k)}^{n} + T_{(i,j+1,k)}^{n} + T_{(i,j-1,k)}^{n} + T_{(i,j,k+1)}^{n} + T_{(i,j,k-1)}^{n}\right) + (1-6\tau)T_{(i,j,k)}^{n} \quad (6)$$

Moreover, the interface described in Eq. (7) is applied in each node, with the contact between the PCM and tube walls within a length differential (L).

$$\kappa_{PCM} A_{PCM} \frac{T_{(i-1,j,k)}^{n} - T_{(i,j,k)}^{n}}{L} + \kappa_{metal} A_{metal} \frac{T_{(i+1,j,k)}^{n} - T_{(i,j,k)}^{n}}{L} = 0 \quad (7)$$

All of the PCM thermo-physical properties utilized to solve the previous equations are temperature independent, but different values are considered in the function of the state (liquid/solid). The state is demarcated by the liquid fraction (*f*), which is defined for each time (*t*) in the function of the PCM melting temperature (T_m) according to Eq. (8) [51] and considering the phase change as an isothermal process. This parameter is important since it defines the portion of PCM melted or solidified, which is the limit condition for the charging process.

$$f_{(i,j,k)}^{n} = \begin{cases} 1 \; if \; T_{(i,j,k)} > T_m \\ f_{(i,j,k)}(t) \; if \; T_{(i,j,k)} = T_m \\ 0 \; if \; T_{(i,j,k)} < T_m \end{cases} \quad (8)$$

Finally, both convection and conduction are considered as the dominant phenomena during the PCM melting and solidification. The effects of natural convection inside the concentric tubes were taken into account during the PCM melting and freezing by utilising an effective conductivity (κ_{eff}) by following Eq. (9) [52]. In this equation, *Pr* is de Prandtl number, *Ra* is the Rayleigh number, D_{int} defines the interior diameter and D_{ext} is the external diameter of the double concentric tubes.

$$\frac{\kappa_{eff}}{\kappa} = 0.386\left(\frac{P_r}{0.861+P_r}\right)^{1/4}\left(\left(\frac{\left[\ln\left(\frac{D_{ext}}{D_{\text{int}}}\right)\right]^4}{\left(\frac{D_{ext}-D_{\text{int}}}{2}\right)^3\left(D_{\text{int}}^{-3/5}+D_{ext}^{-3/5}\right)^5}\right)Ra\right)^{1/4} \quad (9)$$

As a summary of the computational calculation process, Figure 4 represents the steps followed to perform heat transfer and temperature simulation.

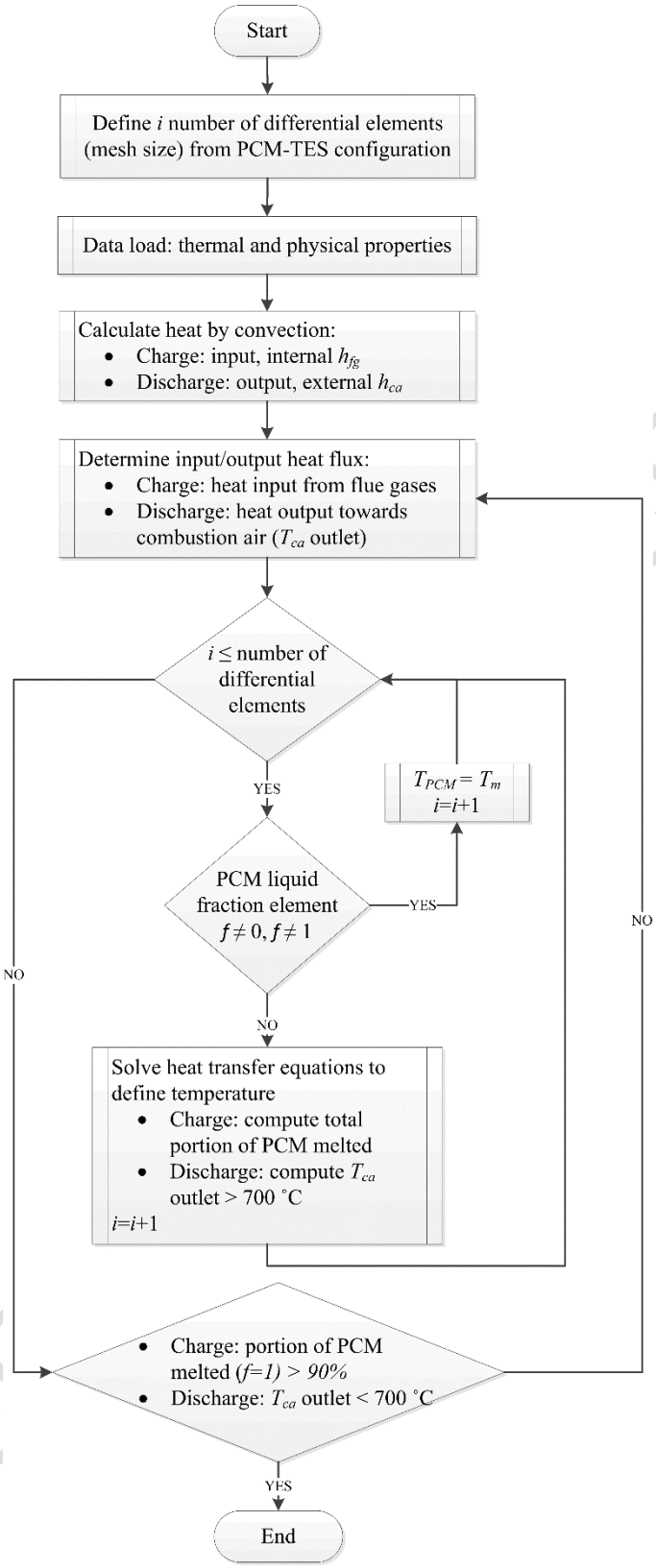

Figure 4. General description of thermal simulation algorithm.

2.3.2 Validation

The developed PCM modelling algorithm is generic and flexible enough to be adaptable any shell-and-tube configuration. Therefore, during the validation phase, the finite difference code was

adjusted to operate exactly under the same operational parameters, PCM thermo-physical properties and boundary conditions established in reference [53]. As a result, a profile temperature is obtained in transient state; which can be directly compared to the experimental data reported in [53], in order to validate the reliability of the results obtained using the in-house developed code. The comparison was performed for one charging cycle in a horizontal-oriented shell and tube heat exchanger, incorporating a medium-temperature PCM (erythritol) with a melting point of 117˚C and a heat of fusion of 340 kJ/(kg·K). The diameter of inner copper tubes is 54 mm where the water is flowing as HTF; while the shell diameter is near 150 mm. the initial temperature of water inlet was 20˚C and it achieved and average output temperature of 61.6˚C. The temperature gradients were compared along the three system directions under the same operating conditions, sizing and geometry parameters.

A cross-section of the tube with the temperature profile following three hours of charging is illustrated in Figure 5. The fluid layer thickness increases from the inside, around the heat transfer tube and towards the more external layers. This behaviour follows a symmetrical dynamic during the melting phase, particularly during the first several hours of the heat transference, when conduction is the dominant mechanism. As time progresses, the natural convection will have progressively more important effects and the profile will not be as symmetrical. The remainder of the PCM remains in the solid phase. Overall, the measured temperatures reported in [53] are very similar compared to this case, only differing by approximately 5˚C, as a maximum. The dissimilarities can be identified mainly at 117 ˚C, at the beginning and end of the phase change.

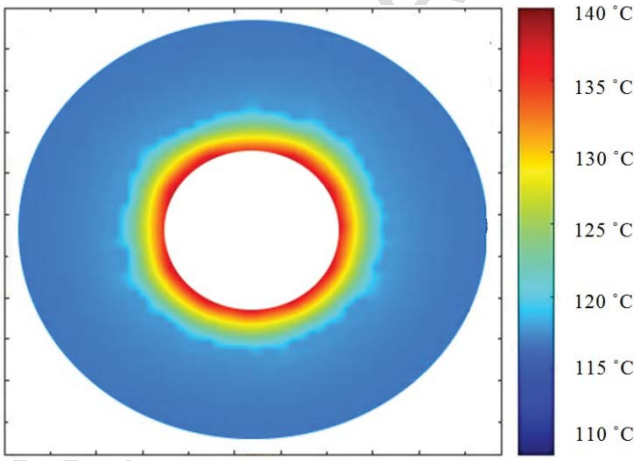

Figure 5. Temperature profile in a cross-section of the PCM tube.

Moreover, Figure 6 illustrates a comparison between the variation of average temperature of the control PCM system, which is calculated from the thermocouple readings in reference [53], and the average simulated temperatures in the same locations along the PCM. Along a five- hour period, the maximum difference exhibits a relative error of 8%. The temperatures from the numerical model simulations are slightly higher than those of the control system. Once the transition is achieved, both temperatures present a very similar curve and remain almost constant during the phase transition dominated by latent heat.

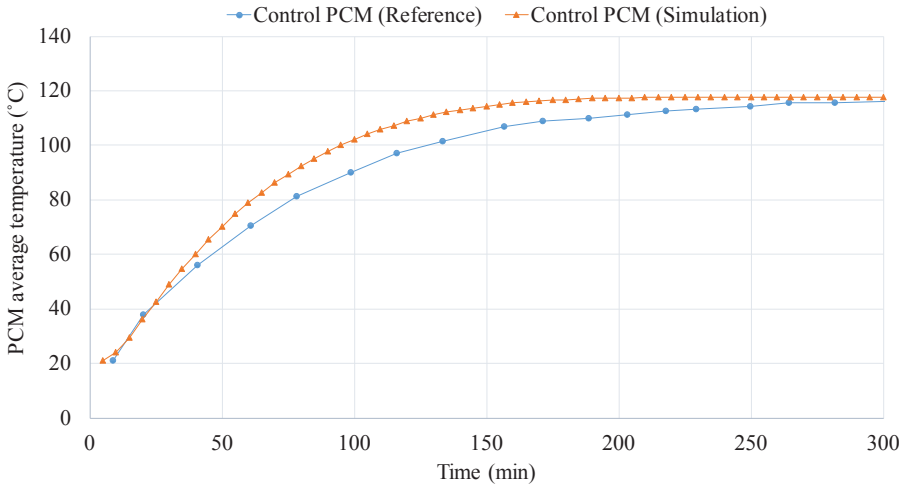

Figure 6. Temperature profile evolution for validating the PCM model.

The differences can be explained by the adiabatic assumption in the numerical model and by the approximation of the spatial and temporal derivative of the heat diffusion equation in the FDM. Furthermore, the thermo-physical properties are assumed to be temperature independent, making the simulated temperature phase change less smooth than the experimental one. In order to achieve a more accurate model, a characterisation of the PCM properties is necessary in the temperature function. In conclusion, a strong agreement is observed between the present developed numerical model simulation and PCM behaviour described in [53], so the modelling is assumed to be satisfactory. Furthermore, this process allowed confirming the robustness and flexibility of the simulation code.

3 Results and discussion

The previously described PCM modelling allows for obtaining the thermal performance of the defined PCM-TES operational and thermo-physical parameters (Table 1). The temperature was calculated for all mesh points, enabling determination of the thermal profiles of the PCM, metal tubes, flue gases and combustion air along the tube length as well as at every time of the entire process. A summary of the most relevant results is presented in this section.

3.1 PCM temperature profile

The simulated temperature profile in the middle of the PCM-TES tube is presented for the charging process in Figure 7. In the first instance (melting 0%), less energy is required to heat the PCM than during the phase transition. Hence, the PCM temperature increases more rapidly before and after the phase change is completed, owing to the sensible heat effect. When the PCM initiates melting, its temperature has already achieved the transition point (885°C) and it absorbs thermal energy by means of latent heat. Following six hours (upper right side of Figure 7), only the closer layers to the inner tube are melted, where flue gases are flowing, while the more external layers remain solid. When the charging time reaches 11 hours, half of the PCM is melted and the temperature profile is more uniform along the thickness. From this time, the liquid PCM expands more homogenously, layer by layer. Following 15 hours, 85% of the PCM is in a liquid state at a temperature of approximately 925°C for the PCM in contact with the inner tube and 885°C near the outer tube, where it is still undergoing a phase change.

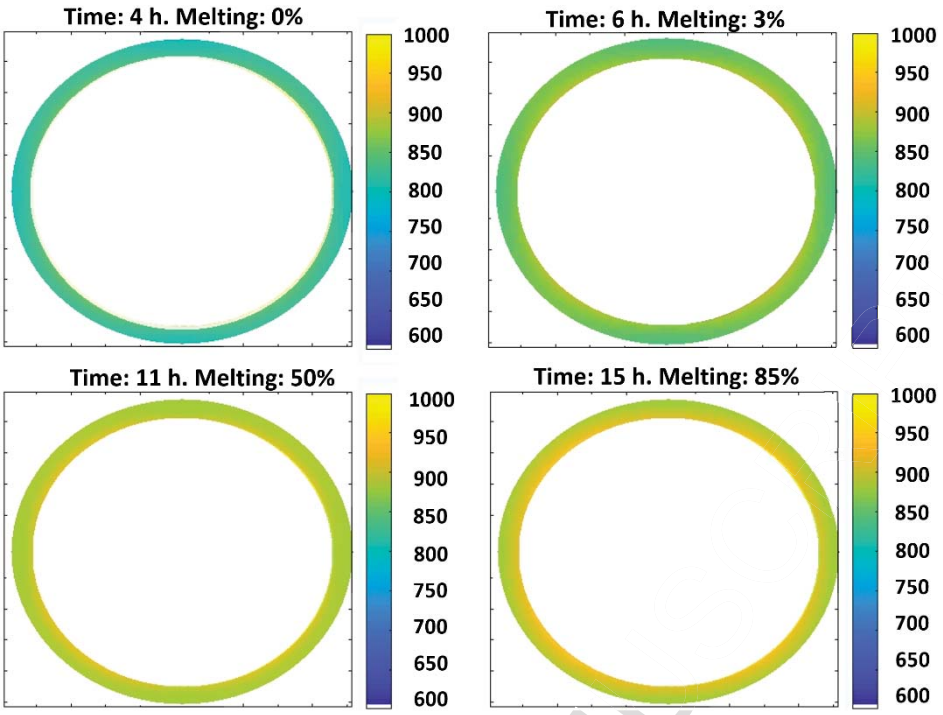

Figure 7. PCM Temperature profile [°C] during charging in the middle of the tube.

Correspondingly, Figure 8 illustrates the temperature profile for the discharge phase in the tube midpoint, as well as the solidification rate at certain relevant times. During the first hours of discharging, the phase transition inside the PCM is very well illustrated in the thermal profile, as different temperature layers are distinguished. In the first hour, the solidification process advances up to 35% and the majority of the PCM thickness reaches the transition temperature until the tube midpoint. After three hours, a substantial amount of PCM is already solidified by releasing the stored heat, and only the inner part of the ring is still in the liquid state, with a temperature above its melting point. The PCM achieves a complete solidification state after five hours. At this time, the combustion air can still exit the PCM-TES at a very high temperature, with values near 800°C. This is because thermal energy exists in terms of sensible heat available in the storage system, which may be useful for the preheating process. Thereafter, the heat transference exhibits a much more homogenous and uniform profile (depicted on the bottom-right side of Figure 8) as the PCM temperature decreases, until it reaches the minimum temperature that is acceptable for the combustion air.

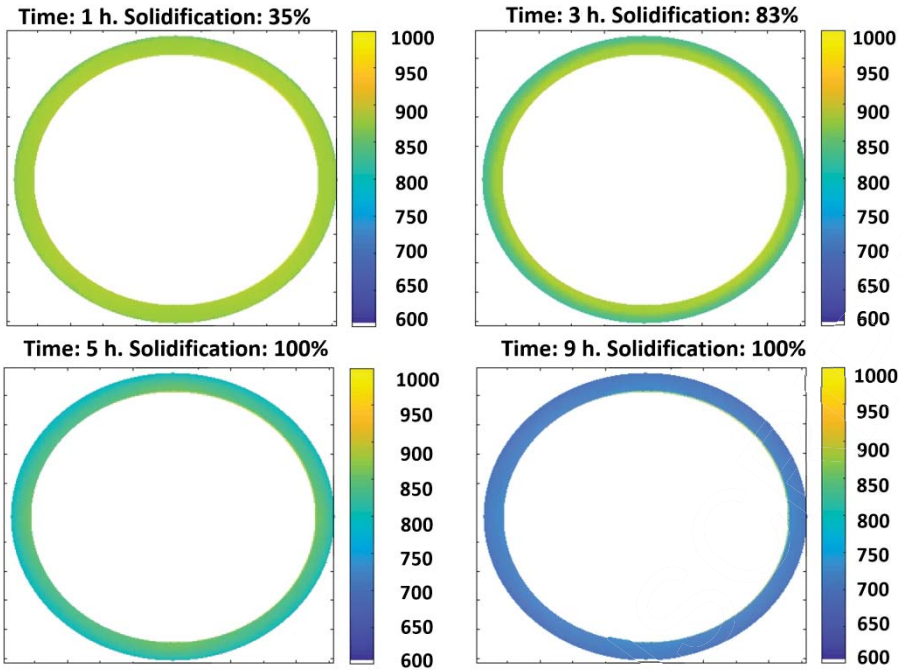

Figure 8. Combustion air and PCM temperature profile [°C] during discharging in the middle of the tube.

3.2 PCM-TES thermal performance and charge/discharge processes

The results gathered in Table 2 indicate the melting/solidification percentages during the charge/discharge processes, respectively. Moreover, the evolution of the combustion air temperature is defined during discharging.

Table 2. Main operational parameters of the PCM-TES.

Time (hours)	Charge (% $_{liquid}$)	Discharge (% $_{solid}$)	$T_{comb\ air}$ (˚C)
1	0	35	865
2	0	63	836
3	0	83	824
4	0	95	811
5	0.5	100	796
6	3	100	771
7	10	100	744
8	19	100	723
9	30	100	**705**
10	39		
11	50		
12	60		
13	70		
14	80		
15	85		
16	**92**		

Once the PCM-TES has recovered the waste heat from the high-temperature exhaust gases, the energy is discharged into the combustion air in order to preheat the stream entering the frit furnace. At the combustion air outlet, the temperature ranges from 865 to 705°C during the whole discharge process. This indicates a relevant increase with reference to the combustion air inlet, which reaches 650°C after passing through a conventional heat exchanger beforehand. At the beginning of the discharging, most of the contribution of the combustion air temperature increase takes place by means of the stored heat as latent heat (70%), while the share of sensible heat (solid state) is substantially smaller. In this sense, the temperature increase can be considered as a nearly isothermal process, as it decreases by only approximately 50°C in four hours. Conversely, the combustion air decreases its temperature by more than 100°C in the following five hours, once the PCM has solidified completely. The PCM temperature decreases under its melting point, thereby reducing the gradient with the combustion air. Along with this gradient reduction, the heat transference rate also decreases, but it still provides a higher temperature with respect to the inlet baseline (650°C) without PCM-TES integration.

The PCM charging process ends after 16 hours, when almost the totality of the material is melted. However, the discharge process should be stopped after nine hours, because at this moment, the temperature of the combustion air will still be over 700°C and the PCM is already 100% in the solid state. In conclusion, a complete cycle of the PCM for charging and discharging lasts for a total of 25 hours. When the discharge phase is over, the cycle is complete and the PCM can start the charge again, absorbing heat while melting and storing the thermal energy.

As a result, the natural gas consumed for feeding the furnace can be reduced, owing to the increase in the combustion air during the discharge phase. Considering an industrial process with no heat recovery at all, the annual savings that a similar plant would achieve accounts for approximately 50000 Nm^3 of natural gas. In that case, the energy saved resulting from to the natural gas savings due to the PCM-TES integration for heat recovery would be approximately 570 MWh on a yearly basis.

Faster and more flexible charging/discharging periods will allow for increasing the PCM-TES adaptability to a wider variety of process integration. In the research for a means to enhance the heat exchange, the combustion air speed and heat exchange area should be maximised in order to increase the convection and overall heat transfer coefficient. Therefore, the discharging time can be reduced without compromising the high temperature achieved for the combustion air at the PCM-TES outlet. In this regard, numerous studies have focused on heat transfer intensification methods, including integration of fins [54], and also other thermal conductivity enhancement techniques, for instance, porous foam or metallic structures, advanced nanomaterial incorporation, micro and macro encapsulation [55]. Furthermore, the use of metal alloys as PCM is also very promising alternative at high temperatures, thanks to their high thermal conductivity, which may significantly reduce the melting and solidification time. However, there is a lack of understanding on the implications of the metallurgical aspects that could risk the implementation of the system [56], mainly due to thermal expansion when encapsulating inside the double concentric tubes, or incompatibility issues under thermal cycling at high temperatures. Since significantly more research is needed, thermal performance parametric analysis, characterization, and stability tests are key aspects for future research before implementing the metal alloys as PCMs in TES at industrial scale.

3.3 Combustion air temperature analysis

For further details on the combustion air, Figure 9 depicts the temperature profile at different tube lengths concretely, at the beginning of the tube, in the midpoint and at the end of the tubes. The latter is the approximate temperature of the combustion air for preheating, as it is the closest point to the PCM-TES outlet. It is worth noting that the curve is considerably more constant during the first several hours, owing to the phase changing effect, with the gradient between the PCM and combustion air inlet. The combustion air temperature increases rapidly owing to the high gradient (around 160°C) in the heat transference during the first hours of discharging. Therefore, the combustion air can reach more than 860°C after two hours of operation. While the PCM undergoes a phase change from liquid to solid, the gradient is maintained and the beginning of the tube firstly solidifies, while the remainder is still in the liquid state. After six hours of discharging, the gradient is reduced to below 50°C at the end of this stage, where the sensible heat is the dominant transference phenomenon. Thereafter, the combustion air decreases as the PCM releases the stored heat until the minimum limit (around 700°C) after nine hours.

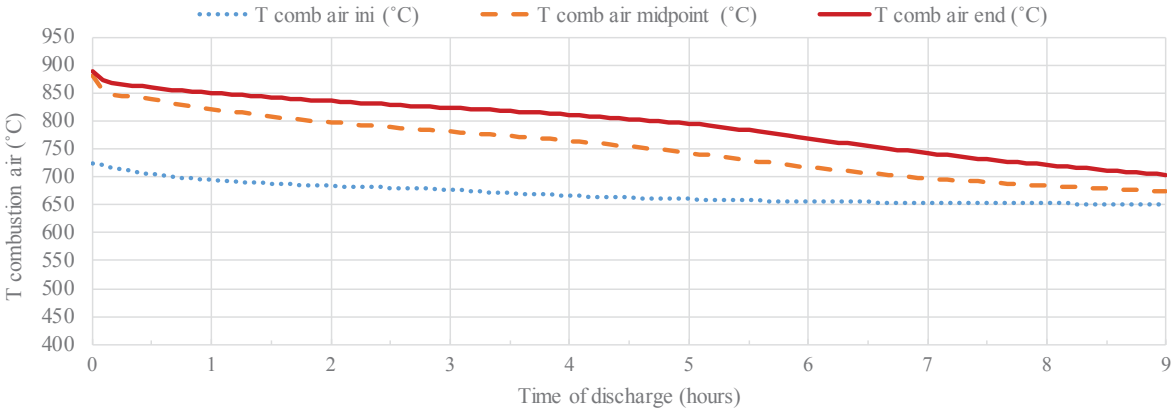

Figure 9. Combustion air temperature behaviour during discharging phase at different tube lengths.

The heat transference inside the PCM-TES is a gradual process along the tube length, but is neither uniform nor linear. The combustion air temperature is analysed in detail for an initial, a middle and an ending point of the tubes, as illustrated in Figure 10. At the beginning of the discharge phase, 50 to 80% of the entire temperature increase is achieved while the combustion air circulates through the first half of the tube. This is because the PCM contained at the beginning of the tube is solidified by releasing the majority of the stored latent heat. For example, the combustion air rapidly increases from 650 to 775°C when passing through 1.5 m during the first hour. Conversely, the growth curve slope is reduced in the following length sections (from 2 m) as the heat transference rate decreases with an approximation to thermal equilibrium, which is depicted by its convex tendency.

However, the curve tendency becomes concave as the discharge continues after the first four hours, when the phase transition is almost completed (95% of the PCM is already solid). From then on, the highest temperature augmentation for the combustion air stream occurs at the end of the tube length, where the PCM temperature is higher. For example, after nine hours of discharging, the temperature increases by approximately 50°C in the second half of the tube length, which means 80% of the total increase. Therefore, when 100% of the PCM is solid, the heat transference rate occurs essentially in the final section of the tube and by means of sensible heat.

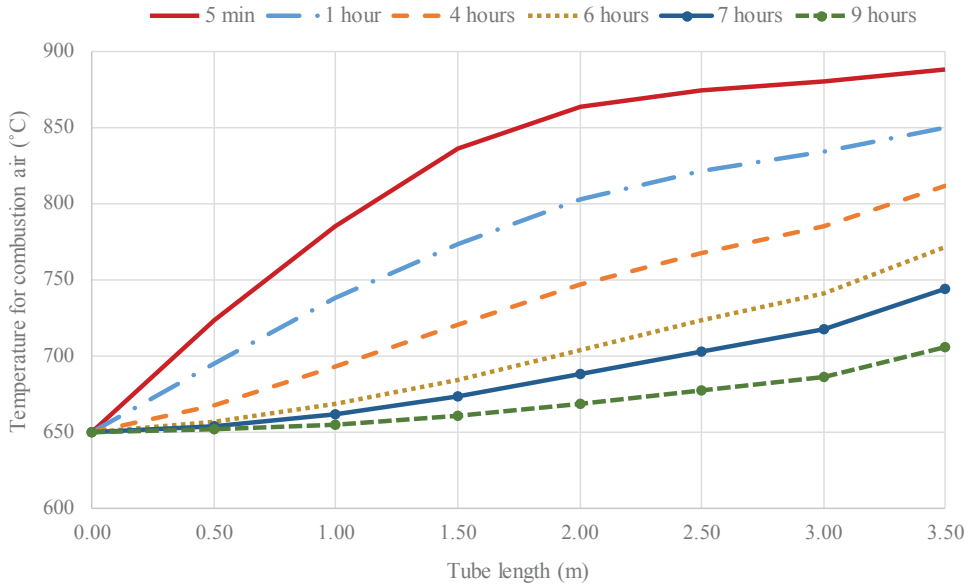

Figure 101. Combustion air temperature behaviour along tube length at different discharging times.

Therefore, Figure 9 and Figure 10 provide useful information regarding the thermal behaviour of not only the combustion air, but also the metal layer in contact with this flow in the external shell. G. Krajačić *et al.* [57] pointed out the necessity of providing an appropriate material for withholding the PCM, resisting all stresses and ensuring safe use. Therefore, the shell design temperature should consider the maximum temperature achieved by the combustion air and maximum gradient. These outputs are relevant for thermomechanical calculations, the stress resistance of metals and possible degradation issues [36]. Apart from this, the temperature profile in the interior of the double concentric tubes should be contentiously analysed in order to predict potential thermal stress risks.

4 Conclusions

At present, working with PCM as a thermal storage and recovery system at high temperatures is both promising and challenging. This study assesses in detail the thermal performance of latent heat thermal storage for industrial integration, by evaluating the thermal profiles, charging/discharging times, portion of PCM solidified/melted and gas flow temperatures (combustion air and exhaust gases). The analysis of these parameters is crucial in the material selection and equipment sizing for its further integration at industrial scale. The 3D numerical modelling for the presented in this study can serve as a first-step implementation of the technology for evaluating the PCM feasibility for heat recovery at very high levels in EIIs. Thus, the main parameters for the PCM system performance and design are defined in the function of the developed model outputs.

A case study in the ceramic industry is presented in detail, with the aim of recovering waste heat at very high temperature levels (over 1100°C) from the furnace exhaust gases. The system configuration consists of an external shell containing double concentric tubes of 2 m long and 600 mm in diameter, filled with 4700 kg of PCM. Consequently, the recovery of waste heat is possible within the temperature range of 700 to 865°C, using a PCM with a melting point around 885°C and considering the proposed PCM-TES design. The temperature increase allows for preheating

the combustion air entering the furnace, and potentially reduces the natural gas consumption and enhances the overall system efficiency. Besides, the charging and discharging time of this PCM-TES are set to approximately 25 hours (16 hours for charging and nine hours for discharging), which is significantly influenced by the low PCM thermal conductivity.

By analysing the temperature profiles, it is found that the combustion air heating is a gradual process along the tube length, but is neither uniform nor linear. The phase transition evolution is presented in detail during both the charge and discharge phases. In this type of system, the majority of the thermal contribution arises from the latent heat owing to the PCM integration, which substantially increases the system heat capacity. This effect is clearly observed within the first several hours of discharging, particularly in the first section of the tube, where 50 to 80% of the temperature increase is achieved. In general, the tube section between 2 and 3 m withstands the highest gradient (maximum around 200°C) during the entire discharge phase. Furthermore, special attention should be paid during the beginning of the charging and discharging, as the temperature changes are strong and may cause thermal stress along the tube.

Based on the work described above, the PCM-TES contributes not only to seeking strategies for waste heat recovery, but also initiates a path for ensuring successful design to be integrated in EII. The predicted system thermal behaviour provides the basis for the PCM-TES design, operational performance and material selection for heat recovery at high temperature ranges. Furthermore, the flexibility of the PCM systems offers the opportunity to adapt the designs depending on the specific plant requirements, thereby increasing its replicability not only in different processes, but also various other EII sectors.

Future work should include a more accurate approximation for natural convection in order to improve the numerical model, particularly according to its importance during melting. Moreover, the implementation of an industrial prototype will validate the simulation results, and refine the developed computational simulation code. Assessing the complete charge/discharge cycles would allow for investigating the PCM-TES behaviour at the industrial level for an improved understanding of the internal flows and detection of critical points from the design and thermomechanical perspectives.

Abbreviations

A	Area (m^2)
ca	sub index for combustion air
c_p	Specific heat (J/(kg·K))
D	Diameter or representative geometrical parameters (m)
ΔT	Increment of temperature (ºC)
EII	Energy Intensive Industry
FDM	Finite Differences Model
f	Liquid/solid fraction (-)
fg	sub index for flue gases
HTF	Heat Transfer Fluid
h_{conv}	Convective heat transfer coefficient (W/(m^2·K))
h_{ca}	Convective heat transfer coefficient in the shell side (W/(m^2·K))
h_{fg}	Convective heat transfer coefficient in the tube side (W/(m^2·K))
i	x-space step (s)
j	y-space step (s)

ACCEPTED MANUSCRIPT

k	z-space step (s)
κ	Thermal conductivity (W/(m·K))
κ_{eff}	Effective Thermal conductivity to consider convection phenomena (W/(m·K))
L	Length differential (m)
n	Iteration step (-)
m	Melting
m_{fg}	flue gas mass flow (kg/h)
Nu	Nusselt number
PCM	Phase Change Materials
Pr	Prandtl number (-)
Q	Heat demand from the process (J/h)
Q_{PCM}	Heat power of the PCM-TES system (W)
Ra	Rayleigh number (-)
Re	Reynolds number (-)ρ Density (kg/m^3)
T	Temperature (ºC)
TES	Thermal Energy Storage
t	Time (s)
τ	Fourier number (-)
U	Overall heat transfer coefficient (W/(m^2·K))

Acknowledgements

The research leading to these results received funding from the European Union H2020 Programme (H2020-SPIRE-2016) under grant agreement no. 723803-VULKANO project. The authors extend their thanks to the project partners for providing support to this research.

Declarations of interest: none.

References

[1] Gao Y, Gao X, Zhang X. The 2 °C Global Temperature Target and the Evolution of the Long-Term Goal of Addressing Climate Change—From the United Nations Framework Convention on Climate Change to the Paris Agreement. Engineering. 2017; 3: 272-278. https://doi.org/10.1016/J.ENG.2017.01.022.

[2] Oettinger GH, Energy roadmap 2050. Office of the European Union, Luxembourg, 2012: 24. 10.2833/10759.

[3] United Nations - Framework Convention on Climate Change (FCCC), Paris Agreement-Decisions adopted by the Conference of the Parties, 2015: 36.

[4] Napp TA, Gambhir A, Hills TP, Florin N, Fennell PS. A review of the technologies, economics and policy instruments for decarbonising energy-intensive manufacturing industries. Renew Sust Energ Rev. 2014; 30: 616-640. 10.1016/j.rser.2013.10.036.

[5] Lund H. Renewable energy strategies for sustainable development. 2007; 32: 912-919. https://doi.org/10.1016/j.energy.2006.10.017.

[6] Royo P, Ferreira VJ, López-Sabirón AM, García-Armingol T, Ferreira G. Retrofitting strategies for improving the energy and environmental efficiency in industrial furnaces: A case study in the aluminium sector. Renew Sust Energ Rev. 2018; 82: 1813-1822. https://doi.org/10.1016/j.rser.2017.06.113.

[7] Krajačić G, Vujanović M, Duić N, Kılkış Ş, Rosen MA, Ahmad Al-Nimr Md. Integrated approach for sustainable development of energy, water and environment systems. Energy Convers Manage. 2018; 159: 398-412. https://doi.org/10.1016/j.enconman.2017.12.016.
[8] Lund H, Østergaard PA, Connolly D, Mathiesen BV. Smart energy and smart energy systems. 2017; 137: 556-565. https://doi.org/10.1016/j.energy.2017.05.123.
[9] Goodman P, Roberston C, Enterprise ECD-Gf, Industry, Limited ET, Service BI. Sustainable Industrial Policy: Building on the Eco-design Directive - Energy-using Products Group Analysis -2- Lot 4: Industrial and Laboratory Furnaces and Ovens - Tasks 1 -7: Final Report. ERA; 2012.
[10] Plisson P, Waste heat recovery: technologically and economically viable solutions for industrial businesses-A white book on industrial waste heat recovery. FIVES, France, 2016.
[11] Papapetrou M, Kosmadakis G, Cipollina A, La Commare U, Micale G. Industrial waste heat: Estimation of the technically available resource in the EU per industrial sector, temperature level and country. Appl Energy. 2018; 138: 207-216. https://doi.org/10.1016/j.applthermaleng.2018.04.043.
[12] Lin Y, Alva G, Fang G. Review on thermal performances and applications of thermal energy storage systems with inorganic phase change materials. 2018; 165: 685-708. https://doi.org/10.1016/j.energy.2018.09.128.
[13] Platform ET. Energy-intensive industries: how we can achieve 'zero carbon' production. www.theclimategroup.org/news/energy-intensive-industries-how-we-can-achieve-zero-carbon-production; 2016 [accesed 05/09/2018].
[14] Bureau of Energy Efficiency. Waste Heat Recovery. Energy Efficiency in Thermal Utilities, India, 2009.
[15] Zhang H, Wang H, Zhu X, Qiu Y-J, Li K, Chen R, et al. A review of waste heat recovery technologies towards molten slag in steel industry. Appl Energy. 2013; 112: 956-966. https://doi.org/10.1016/j.apenergy.2013.02.019.
[16] López-Sabirón AM, Royo P, Ferreira VJ, Aranda-Usón A, Ferreira G. Carbon footprint of a thermal energy storage system using phase change materials for industrial energy recovery to reduce the fossil fuel consumption. Appl Energy. 2014; 135: 616-624. http://dx.doi.org/10.1016/j.apenergy.2014.08.038.
[17] Zhang HL, Baeyens J, Degreve J, Caceres G, Segal R, Pitie F. Latent heat storage with tubular-encapsulated phase change materials (PCMs). Energy. 2014; 76: 66-72. 10.1016/j.energy.2014.03.067.
[18] Mahdi JM, Lohrasbi S, Ganji DD, Nsofor EC. Accelerated melting of PCM in energy storage systems via novel configuration of fins in the triplex-tube heat exchanger. Int J Heat Mass Transfer. 2018; 124: 663-676. https://doi.org/10.1016/j.ijheatmasstransfer.2018.03.095.
[19] Nomura T, Tsubota M, Oya T, Okinaka N, Akiyama T. Heat storage in direct-contact heat exchanger with phase change material. Appl Therm Eng. 2013; 50: 26-34. 10.1016/j.applthermaleng.2012.04.062.
[20] Sharma A, Tyagi VV, Chen CR, Buddhi D. Review on thermal energy storage with phase change materials and applications. Renew Sust Energ Rev. 2009; 13: 318-345. 10.1016/j.rser.2007.10.005.
[21] Zalba B, Marin JM, Cabeza LF, Mehling H. Review on thermal energy storage with phase change: materials, heat transfer analysis and applications. Appl Therm Eng. 2003; 23: 251-283. Pii S1359-4311(02)00192-8
Doi 10.1016/S1359-4311(02)00192-8.
[22] Kenisarin MM. Thermophysical properties of some organic phase change materials for latent heat storage. A review. Sol Energy. 2014; 107: 553-575. 10.1016/j.solener.2014.05.001.

[23] Kenisarin MM. High-temperature phase change materials for thermal energy storage. Renew Sust Energ Rev. 2010; 14: 955-970. http://dx.doi.org/10.1016/j.rser.2009.11.011.
[24] Ferreira VJ, López-Sabirón AM, Royo P, Aranda-Usón A, Ferreira G. Integration of environmental indicators in the optimization of industrial energy management using phase change materials. Energy Convers Manage. 2015; 104: 67-77. http://dx.doi.org/10.1016/j.enconman.2015.05.011.
[25] Frazzica A, Palomba V, La Rosa D, Brancato V. Experimental comparison of two heat exchanger concepts for latent heat storage applications. Enrgy Proced. 2017; 135: 183-192. 10.1016/j.egypro.2017.09.501.
[26] Li M-J, Jin B, Ma Z, Yuan F. Experimental and numerical study on the performance of a new high-temperature packed-bed thermal energy storage system with macroencapsulation of molten salt phase change material. Appl Energy. 2018; 221: 1-15. https://doi.org/10.1016/j.apenergy.2018.03.156.
[27] Seddegh S, Joybari MM, Wang XL, Haghighat F. Experimental and numerical characterization of natural convection in a vertical shell-and-tube latent thermal energy storage system. Sustain Cities Soc. 2017; 35: 13-24. 10.1016/j.scs.2017.07.024.
[28] Bayón R, Rojas E, Valenzuela L, Zarza E, León J. Analysis of the experimental behaviour of a 100 kW latent heat storage system for direct steam generation in solar thermal power plants. 2010; 30: 2643. 10.1016/j.applthermaleng.2010.07.011.
[29] Garcia P, Olcese M, Rougé S. Experimental and Numerical Investigation of a Pilot Scale Latent Heat Thermal Energy Storage for CSP Power Plant. 2015; 69: 842-849. https://doi.org/10.1016/j.egypro.2015.03.102.
[30] Hoshi A, Mills D, Bittar A, S. Saitoh T. Screening of high melting point phase change materials (PCM) in solar thermal concentrating technology based on CLFR; 2005. 10.1016/j.solener.2004.04.023.
[31] Laing D, Bauer T, Breidenbach N, Hachmann B, Johnson M. Development of high temperature phase-change-material storages. 2013; 109: 497-504. http://dx.doi.org/10.1016/j.apenergy.2012.11.063.
[32] Bie Y, Li M, Chen F, Królczyk G, Yang L, Li Z, et al. A Novel Empirical Heat Transfer Model for A Solar Thermal Storage Process using Phase Change Materials. 2018. https://doi.org/10.1016/j.energy.2018.11.107.
[33] Pirasaci T, Wickramaratne C, Moloney F, Goswami DY, Stefanakos E. Influence of design on performance of a latent heat storage system at high temperatures. Appl Energy. 2018; 224: 220-229. https://doi.org/10.1016/j.apenergy.2018.04.122.
[34] Du K, Calautit J, Wang Z, Wu Y, Liu H. A review of the applications of phase change materials in cooling, heating and power generation in different temperature ranges. 2018; 220: 242-273. https://doi.org/10.1016/j.apenergy.2018.03.005.
[35] Castell A, Solé C. An overview on design methodologies for liquid–solid PCM storage systems. Renew Sust Energ Rev. 2015; 52: 289-307. https://doi.org/10.1016/j.rser.2015.07.119.
[36] Bengt Sunden, High Temperature Heat Exchangers (HTHE) in: M.I. R.K. Shah, T.M. Rudy, V.V. Wadekar, (Ed.). 5th International Conference on Enhanced, Compact and Ultra-Compact Heat Exchangers: Science, Engineering and Technology, New Jersey, USA, 2005.
[37] Yang K, Zhu N, Chang C, Wang D, Yang S, Ma S. A methodological concept for phase change material selection based on multi-criteria decision making (MCDM): A case study. 2018; 165: 1085-1096. https://doi.org/10.1016/j.energy.2018.10.022.
[38] Navarrete N, Mondragón R, Wen D, Navarro ME, Ding Y, Juliá JE. Thermal energy storage of molten salt –based nanofluid containing nano-encapsulated metal alloy phase change materials. 2019; 167: 912-920. https://doi.org/10.1016/j.energy.2018.11.037.

[39] Agyenim F, Eames P, Smyth M. A comparison of heat transfer enhancement in a medium temperature thermal energy storage heat exchanger using fins. Sol Energy. 2009; 83: 1509-1520. https://doi.org/10.1016/j.solener.2009.04.007.
[40] Horbaniuc B, Dumitrascu G, Popescu A. Mathematical models for the study of solidification within a longitudinally finned heat pipe latent heat thermal storage system. Energy Convers Manage. 1999; 40: 1765-1774. Doi 10.1016/S0196-8904(99)00069-2.
[41] Papanicolaou E, Belessiotis V. Transient natural convection in a cylindrical enclosure at high Rayleigh numbers. Int J Heat Mass Transfer. 2002; 45: 1425-1444. https://doi.org/10.1016/S0017-9310(01)00258-7.
[42] Fukai J, Hamada Y, Morozumi Y, Miyatake O. Improvement of thermal characteristics of latent heat thermal energy storage units using carbon-fiber brushes: experiments and modeling. Int J Heat Mass Transfer. 2003; 46: 4513-4525. https://doi.org/10.1016/S0017-9310(03)00290-4.
[43] Ghoneim AA. Comparison of Theoretical-Models of Phase-Change and Sensible Heat-Storage for Air and Water-Based Solar Heating-Systems. Sol Energy. 1989; 42: 209-220. Doi 10.1016/0038-092x(89)90013-3.
[44] Yousufuddin S, Al-Bazzaz M, Al-Zurayqi M, Al-Yami F. Design and Optimization of a Shell and Tube Heat Exchanger with Different Baffle Spacing Arrangement for Cooling Lean Diethanolamine; 2018. 10.13140/RG.2.2.35836.80003.
[45] Labbadlia O, Laribi B, Chetti B, Hendrick P. Numerical study of the influence of tube arrangement on the flow distribution in the header of shell and tube heat exchangers. Appl Energy. 2017; 126: 315-321. https://doi.org/10.1016/j.applthermaleng.2017.07.184.
[46] Ferziger JH PM. Computational methods for fluid dynamics. 3rd ed. Springer, Berlin; 2002.
[47] John A. Dec RDB, Ablative Thermal Response Analysis Using the Finite Element Method, 47th AIAA Aerospace Sciences Meeting Including The New Horizons Forum and Aerospace Exposition, Orlando, Florida, 2009.
[48] Häggblad J, Runborg O. Accuracy of staircase approximations in finite-difference methods for wave propagation. 2014; 128: 741-771. 10.1007/s00211-014-0625-1.
[49] Mazumder S. Numerical Methods for Partial Differential Equations. Elservier; 2016.
[50] Acevedo L, Usón S, Uche J. Numerical study of cullet glass subjected to microwave heating and SiC susceptor effects. Part I: Combined electric and thermal model. Energy Convers Manage. 2015; 97: 439-457. https://doi.org/10.1016/j.enconman.2015.03.053.
[51] Ciulla G, Lo Brano V, Cellura M, Franzitta V, Milone D, A finite difference model of a PV-PCM system, 1st International Conference on Solar Heating and Cooling for Buildings and Industry2012; 30: 198-206. 10.1016/j.egypro.2012.11.024.
[52] Çengel YA. Heat and mass transfer. McGraw-Hill; 2007.
[53] Agyenim F, Eames P, Smyth M. Heat transfer enhancement in medium temperature thermal energy storage system using a multitube heat transfer array. Renew Energ. 2010; 35: 198-207. 10.1016/j.renene.2009.03.010.
[54] Diao YH, Wang S, Zhao YH, Zhu TT, Li CZ, Li FF. Experimental study of the heat transfer characteristics of a new-type flat micro-heat pipe thermal storage unit. 2015; 89: 871-882. https://doi.org/10.1016/j.applthermaleng.2015.06.070.
[55] Bose P, Amirtham VA. A review on thermal conductivity enhancement of paraffinwax as latent heat energy storage material. Renew Sust Energ Rev. 2016; 65: 81-100. https://doi.org/10.1016/j.rser.2016.06.071.
[56] Fernández AI, Barreneche C, Belusko M, Segarra M, Bruno F, Cabeza LF. Considerations for the use of metal alloys as phase change materials for high temperature applications. 2017; 171: 275-281. https://doi.org/10.1016/j.solmat.2017.06.054.

ACCEPTED MANUSCRIPT

[57] Krajačić G, Duić N, Vujanović M, Kılkış Ş, Rosen MA, Al-Nimr MdA. Sustainable development of energy, water and environment systems for future energy technologies and concepts. Energy Convers Manage. 2016; 125: 1-14. https://doi.org/10.1016/j.enconman.2016.08.050.

ACCEPTED MANUSCRIPT

ACCEPTED MANUSCRIPT

HIGHLIGTHS

- A thermal energy storage based on PCM is proposed to recover high temperature heat.
- An energy intensive industry study case reached a temperature increase up to 200°C.
- 3D-numerical model assesses the thermal behaviour of the waste heat recovery system.
- Combustion air temperature profiles are analysed during charging and discharging.
- A basis is set for system design, thermal stress resistance and material selection.

ACCEPTED MANUSCRIPT